A Model of Transdermal Drug Delivery through Electroporation

Keywords: electroporation, transdermal, drug delivery, stratum corneum, local transport region

BEE 4530: Computer-Aided Engineering: Applications to Biological Processes

James Adair, Emily Chou, Matt Metzloff, Truman Tse

Contents

1 Executive Summary

Electroporation is a technique that applies high voltage pulses over short time periods, resulting in strong electric fields, to create micropores in cell membranes. When applied to the skin, electroporation causes Joule heating that creates local transport regions (LTRs) in the lipid bilayer of the stratum corneum (SC), which is the outermost layer of the epidermis that is most resistant to drug transport. The combined effect of micropores and LTR formation results in a significant increase in transdermal drug transport.

Previous studies only model the drug profile through the skin layers during the electric pulse, on the scale of 300 ms. Furthermore, previous studies only account for a pore that crosses the SC, not the epidermis and dermis. Based on the anatomy of hair follicles and sweat glands, more accurate models should model pores that extend past the SC.

We used COMSOL Multiphysics®: a finite element analysis, solver, and multiphysics simulation software for our modeling. We modeled transdermal delivery of a DNA-based drug assisted by electroporation, using skin property values determined by in vitro studies for large charged molecules. The model covered 24 hours starting with a 300 ms electric pulse. Our cylindrical geometry accounts for the gel, SC, epidermis, and dermis. At the axis of the cylinder, a pore extends through all the skin layers, containing the gel with the drug. We modeled Joule heating that results in LTR formation, as well as the mass transfer during and after the pulse.

Our results demonstrate LTR formation during electroporation and its lasting impact after 24 hours. The concentration of drug at 24 hours decreases going down the LTR in the SC, with a slower decline in the epidermis and dermis. We validated our model through a mesh convergence analysis, comparison with another computational model, and comparison with an experimental study. Through a sensitivity analysis, we reinforced the importance of SC thickness in slowing drug transport.

This model can be used as a more accurate representation of electroporation as a proof of concept before clinical trials.

2 Introduction

Transdermal drug delivery was first approved by the Food and Drug Administration in 1979 for motion sickness. In traditional transdermal delivery methods, drug molecules enter healthy skin cells by passive diffusion [2] [4]. The drug first penetrates the stratum corneum (SC), which is the least permeable layer of the skin. It then passes through the deeper epidermis and dermis layers. Once it reaches the dermis layer, the drug is available for absorption through blood circulation [7]. In addition to its painlessness, advantages of this delivery method include reduced waste, low cost, localized treatment, and preferability for self-administration [3] [8]. However, the SC is a major challenge for transdermal drug delivery, owing to its incredibly low diffusion coefficient. Because of these barrier properties, only a few specific drugs can successfully be delivered transdermally using traditional passive methods - these drugs must have lipid properties but be relatively soluble in water [4].

Since the 1980s, several methods of device-assisted transdermal delivery have been developed, broadening the applications of the method. Device assistance helps facilitate the transport of compounds across the SC and lower layers by mechanisms other than diffusion, allowing many classes of drugs to be delivered more quickly [4]. DNA-based drugs are one such class - they have been of considerable interest in the last decade and have recently been approved for use in the US. They can be used to insert healthy genes into cells or to interfere with disease-causing genes [5]. Current DNA-based drugs have not been delivered transdermally, but researchers are interested in novel methods of delivering them. As research continues on DNA-based drugs, transdermal delivery could be a useful method.

Two existing methods of device-assisted transdermal drug delivery are sonophoresis and iontophoresis. Sonophoresis uses ultrasound to generate heat, changing SC structure to enhance drug penetration [4]. However, sonophoresis treatment can take a long time to administer and requires an intact and healthy SC in order to function, limiting the applicable situations [6]. Iontophoresis uses a low-intensity electric current to transport ionic molecules across the skin, but it can cause skin irritation and damage [9]. There is also inconsistent success between drugs, as iontophoresis is most relevant for delivering charged drugs with small molecular weights [4].

A third method that offers unique advantages is electroporation, which involves applying short high-voltage electrical pulses to the skin. The pulses create micropores in skin cells, leading to significant increases in molecular drug diffusivity [4]. In addition, electroporation causes the skin to increase in temperature and develop Local Transport Regions (LTRs). LTRs are large regions of increased diffusion across the SC that form around pre-existing pores such as sweat glands or hair follicles, through which substantial drug delivery occurs [12]. By optimizing the timing and voltage of the pulses, electroporation can be adapted to deliver many different drugs, including large charged macromolecules such as DNA [10]. Compared to iontophoresis and sonophoresis, electroporation may be the ideal device-assisted method for DNA drug

delivery since it would allow DNA molecules, which are large and charged, to diffuse through the SC via LTRs and into cells through micropores.

There are few models in literature of skin electroporation. Of the published models, none study long-term drug diffusion through the human SC, epidermis, and dermis. In this study, we have analyzed the electroporation-assisted delivery of a DNA drug across human skin. We have modeled the Joule heating that causes LTR formation as well as the mass transfer that occurs after electrophoresis, determining the time-varying concentration gradient of the drug throughout the skin.

2.1 *Problem Statement*

We used COMSOL to perform 2D-axisymmetric modeling of skin electroporation and drug delivery through the stratum corneum, epidermis, and dermis. The model covered 24 hours starting with the electric pulse. The primary aim of our research was to learn about the effect of electroporation on the profile of transdermal drug concentration over large time periods.

2.2 *Design Objectives*

Our study had three primary objectives. We expected these objectives to help in designing a study that would be useful, valid, and significant.

1. As our first objective, we studied the heat transfer and mass transfer that occurs during the electric pulse. As a result of the heating, the model determined the SC lipid melt fraction which dictates the formation of the LTR. This section of the problem modeled the first 300 ms of electroporation.

2. As our second objective, after LTR formation, we only modeled mass transfer in the electroporated skin over the following twenty-four hours. In both sections of the problem, we developed concentration profiles of the diffused drug. The purpose was to show how electroporation affects drug diffusion through the skin at a time scale that is useful for medical purposes.

3. As our third objective, when model validation was complete, we performed sensitivity analysis on the pore radius, the SC diffusion coefficient, and SC thickness to determine the effect of realistic variations on the amount of drug diffused.

3 Problem Formulation

3.1 *Process Description*

In order to be absorbed into the bloodstream, a drug must cross all layers of the skin: the stratum corneum (SC), epidermis, and dermis. The SC is the layer which is most resistant to environmental processes like heat conduction and solute diffusion. It is made up of layers of cells called corneocytes, with lipids filling the gaps between layers. Skin electroporation starts by applying a drug-containing gel to a fold of skin, which is placed between two electrodes, shown in Figure 1.

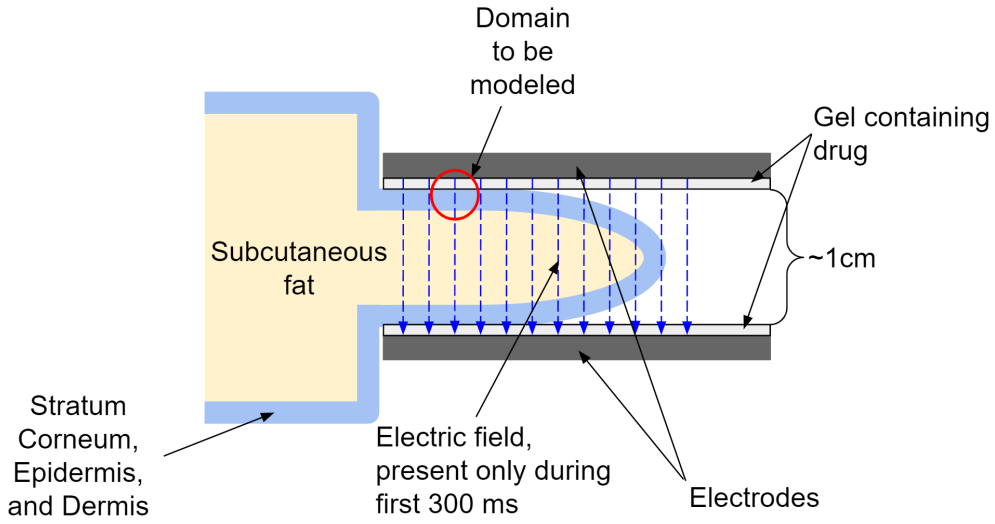

Figure 1: System for Transdermal Drug Delivery with Electroporation. A fold of skin is covered in a drug-containing gel and placed between two electrodes. We modeled a small domain including all layers of the skin, as indicated.

The gel enters pre-existing pores in the SC such as sweat glands or hair follicles, and an electric field is applied for 300 ms. Due to the difference in electrical conductivity between the gel and SC, Joule heating occurs, causing a phase change in the SC lipids. The area around the pre-existing pore in which this phase change occurs is called a local transport region (LTR), and these regions have highly increased drug diffusion rates. After the electric field is applied, the fold of skin is removed from the electrodes and the gel remains on the skin. Because the LTR remains for hours after the pulse ends, drug diffusion remains high after the electric pulse. In addition, electroporation increases the diffusion rate through the epidermis and dermis. The model covered the formation of the LTR during the pulse, and the diffusion of a model drug through all layers of skin over the next twenty-four hours. The model was centered around a single LTR. In Figure 2 we represent the pulse and show a simplified, 2D representation of the skin layers.

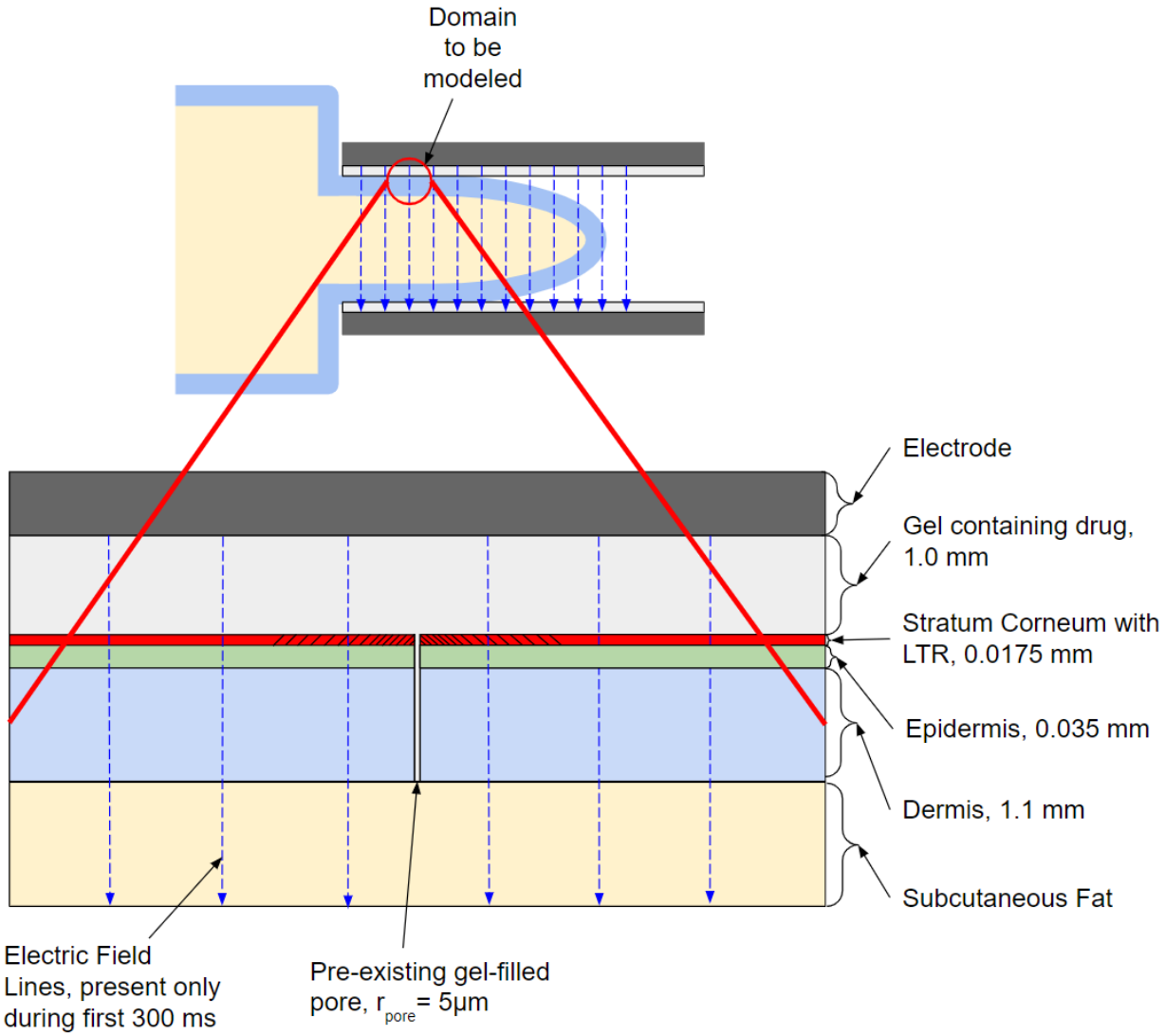

Figure 2: Simplified Domain During Electric Pulse. The simplified domain includes a pre-existing gel-filled pore (either a sweat gland or hair follicle) in the SC, epidermis, and dermis. During the first 300 ms, a 300 V electric field is present. The difference in electrical conductivity between the pore and SC causes joule heating in the SC, which leads to LTR formation. Drug transport occurs from the gel into the skin by electrophoresis and diffusion during the pulse, and by diffusion only after the pulse.

The cylindrical model was simplified as a 2D axisymmetric geometry. The following assumptions were used for our geometric setup:

1. The radial boundaries are thermally insulated.
2. A convective boundary condition is imposed on the upper gel surface.
3. The domain has an initial temperature equal to the arterial blood temperature.
4. There is no electric conduction at the outer radial sides.
5. There is no flux in solute at the radial boundaries of the domain.

6. There is a zero concentration boundary condition at the bottom of the dermis.
7. No solute is transported from the upper gel surface.
8. Metabolic heat generation is neglected.
9. No drug degradation or consumption occurs.

We set the concentration of DNA drug to be zero at the bottom of the dermis to account for drug uptake into the bloodstream. Since there is a large amount of blood and lymphatic vessels at the bottom of the dermis, we assumed that the drug concentration in this boundary is zero, as any drug that reaches this boundary is nearly instantly carried away through circulation [1].

We are able to neglect metabolic heat generation because during and immediately after the 300 ms electric pulse, its contribution is small compared to the heat supplied by Joule heating. Assuming an average human metabolic heat generation rate of 1000 W/m^3, around 2 μJ of heat is delivered to our system in 300 ms. This amount of heat does not cause any significant heating. We did not model heat transfer after 0.3 s, where the contribution from metabolic heat generation becomes more significant, since the purpose of heat transfer calculations was to help model the change in the SC's properties due to the lipid structure phase change that occurs during electroporation. For the time of interest after the pulse, the LTR does not degenerate, and temperature does not affect any properties related to mass transfer.

Figure 3 describes our simplified modeling domain, where we represented the gel, SC, epidermis, and dermis layers surrounding one pre-existing pore.

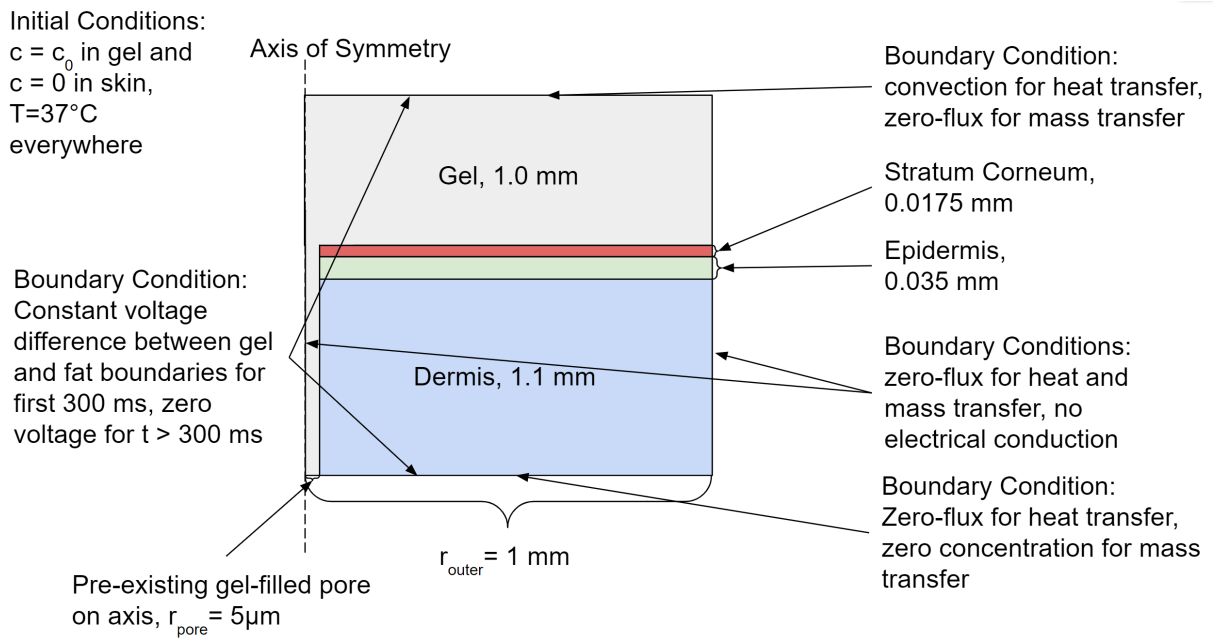

Figure 3: COMSOL Modeling Domain. The axis of symmetry runs through the pre-existing pore. All layers and dimensions are indicated. Initial and boundary conditions are indicated and are further detailed in section 3 below.

This model assumed that hair follicles and sweat glands are distributed relatively evenly across the skin to be electroporated, so that the drug transfer through a single LTR applies to any of the LTRs that are formed. When considering a single LTR, the modeling domain is unaffected by the flattening of the skin fold that occurs when the electrodes are removed after the pulse.

3.2 *Governing Equations - Heat Transfer*

Our model incorporates several forms of heat transfer during the first 300 ms. Equation 1 represents the transient, conduction, perfusion, and Joule heating terms of our heat transfer governing equation:

$$\rho_i c_{p,i} \frac{\partial T}{\partial t} = \nabla \cdot (k_i \nabla T) - \omega_i c_b (T - T_a) + Q_J \quad (1)$$

where T is temperature, t is time, ω_i is non-directional blood flow associated with perfusion, c_b is specific heat of blood, $c_{p,i}$ is specific heat capacity, ρ_i is density, k_i is thermal conductivity, T_a is arterial blood temperature, and Q_J is Joule heat generated from the induced electric field. Joule heat is defined in Equation 2:

$$Q_J = \sigma_i |\nabla \Phi|^2 \quad (2)$$

where $\Phi$is the electric potential of the applied electric field σ_i is electrical conductivity. The subscript *i* is used in the equations to differentiate the properties between different layers of skin.

3.3 *Initial and Boundary Conditions - Heat Transfer*

Equation 3 defines the initial temperature everywhere as uniform and equal to the arterial blood temperature.

$$T|_{t=0} = T_a \quad (3)$$

Equation 4 is a convective boundary condition on the gel surface:

$$-k \frac{dT}{dz}\Big|_{z=3.3525mm} = h(T - T_\infty) \quad (4)$$

where h is the convective heat transfer coefficient, T is the surface temperature, and $T_\infty$is the ambient air temperature.

Equation 5 is a zero flux boundary condition on the bottom as well as the inner and outer radial sides.

$$-k \frac{dT}{dr}\Big|_{r=1mm} = -k \frac{dT}{dr}\Big|_{r=0mm} = -k \frac{dT}{dz}\Big|_{z=0} = 0 \quad (5)$$

3.4 *Governing Equations - Electric Field*

We modeled the electric field that induces Joule heating and electrophoretic mass transfer during the first 300 ms. Equation 6 relates electrical conductivity and potential:

$$\nabla \cdot (\sigma_i \nabla \Phi) = 0 \tag{6}$$

This electric field is only present during the first 300 ms, during which the pulse is applied.

3.5 *Initial and Boundary Conditions - Electric Field*

Equation 7 shows that there is a zero conduction boundary condition on the outer radial sides while the electric field is present. Since the model is axisymmetric there is a zero conduction boundary condition along the inner radial side.

$$\frac{\partial \Phi}{\partial r}\Big|_{r=0mm} = \frac{\partial \Phi}{\partial r}\Big|_{r=1mm} = 0 \tag{7}$$

Equation 8 shows that the top electrode is 300V higher than the bottom electrode during the pulse, leading to an average electric potential gradient of 150 V across each of the two layers of skin in the fold. Our model covered one layer of gel and skin, with a constant voltage difference between the top and bottom surface.

$$(\Phi|_{z=3.3525mm} - \Phi|_{z=0})_{t\leq 300ms} = 150\ V \tag{8}$$

Equation 9 shows the voltage is the same throughout the domain after the pulse, allowing the top and bottom surfaces of the domain to have a constant zero voltage condition.

$$(\Phi|_{z=3.3525mm} - \Phi|_{z=0})_{t>300ms} = 0 \tag{9}$$

3.6 *Governing Equations - Mass Transfer*

Equation 10 is a governing equation that includes mass transfer through the gel, epidermis, and dermis by diffusion with electrophoresis during the pulse:

$$\frac{\partial C}{\partial t} - \nabla \cdot (m_i C \nabla \Phi) = \nabla \cdot (D_i \nabla C) \tag{10}$$

where C is concentration, m_i is electrophoretic mobility of the drug, and D_i is the diffusion coefficient of the drug. Velocity due to electrophoresis is given by $-m_i \nabla \Phi$.

We modeled mass transfer through the SC in a porous media context using Equation 11. This is because the structure of the SC can be described using a brick and mortar model, where the corneocytes are analogous to bricks, and the lipid between the corneocytes are analogous to mortar. Mass transport occurs only within the lipid filled spaces between the corneocytes. The SC required a separate governing equation which accounted for porosity and tortuosity:

$$\frac{\partial C}{\partial t} - \frac{\epsilon_{SC}}{\tau_{SC}}\nabla \cdot (m_L C \nabla \Phi) = \frac{\epsilon_{SC}}{\tau_{SC}}\nabla \cdot (D_L \nabla C) \tag{11}$$

where C is concentration, ϵ_{SC} is porosity of the SC structure, and τ_{SC} is tortuosity of the SC structure.

3.7 *Initial and Boundary Conditions - Mass Transfer*

Equation 12 and 13 include the concentration profile at the beginning of our model. Initially, solute concentration is zero everywhere except the gel layer and the gel filling the pore. The gel has a solute concentration of C_0.

$$C|_{t=0} = 0 \tag{12}$$

$$C|_{t=0,\ 2.3525mm \leq z \leq 3.3525mm} = C_0 \tag{13}$$

Equation 14 shows that there is a zero flux boundary condition at the top and the outer radial sides, and since the model is axisymmetric there is a zero flux boundary condition along the inner radial side.

$$-D\frac{dC}{dr}|_{r=1mm} = -D\frac{dC}{dr}|_{r=0} = -D\frac{dC}{dr}|_{z=3.3525mm} = 0 \tag{14}$$

Equation 15 shows that there is a zero concentration boundary condition at the bottom surface of the dermis.

$$C|_{z=0} = 0 \tag{15}$$

3.8 *SC Lipid Phase Change*

As electroporation occurs, the SC undergoes a phase change in the lipid structure, causing it to lose its tight lamellar framework and altering its properties. The phase change begins once temperature in the SC reaches T_{E1}, and the SC becomes fully transformed after reaching T_{E2}. During this transition, we modeled changes in the SC's properties similarly to methods used to model melting over a temperature range, by using a lipid melt fraction, ϕ, as shown below in equation 16 and figure 4.

$$\varphi = \begin{cases} 0 & : T \le T_{E_1} \\ \frac{T - T_{E_1}}{T_{E_2} - T_{E_1}} & : T_{E_1} < T < T_{E_2} \\ 1 & : T_{E_2} \le T \end{cases} \tag{16}$$

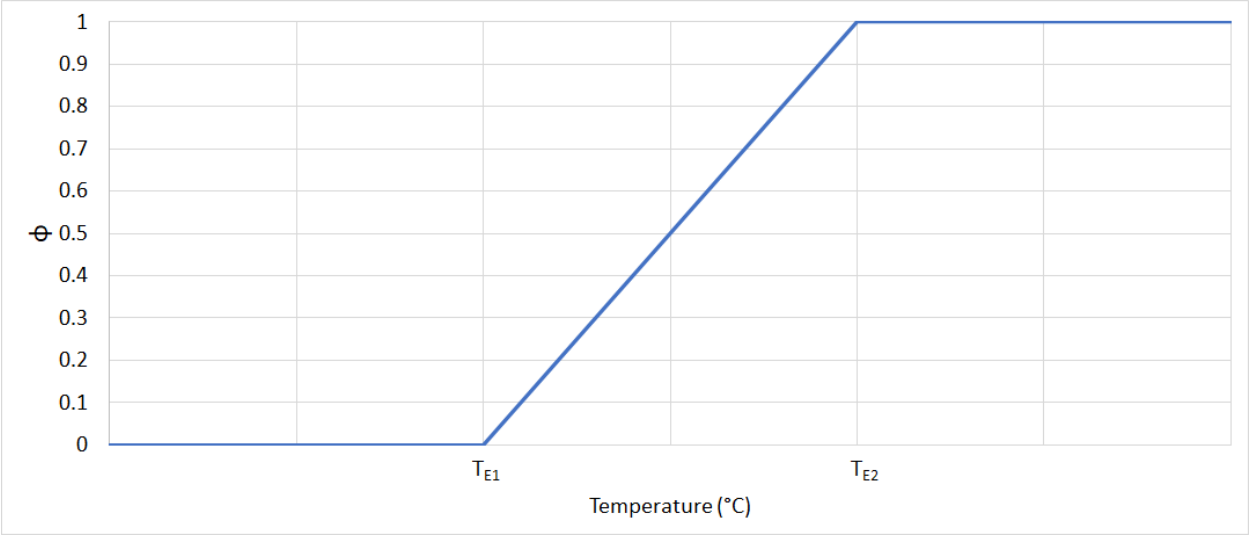

Figure 4. A plot of the lipid melt fraction as a function of temperature. Below T_{E1}, no lipid melting has occurred. Melting occurs linearly between T_{E1} and T_{E2}. Above T_{E2}, full melting has occurred.

Equations 17, 18, and 19 demonstrate the variables that change as a function of temperature, given by the lipid melt fraction. Changes in the electrical conductivity, electrophoretic mobility, and diffusion constant was assumed to have a linear dependence on the lipid melt fraction as shown in the relations:

$$\sigma_{SC} = \sigma_{SC,U} + \phi(\sigma_{SC,M} - \sigma_{SC,U}) \tag{17}$$

$$m_L = m_{L,U} + \phi(m_{L,M} - m_{L,U}) \tag{18}$$

$$D_L = D_{L,U} + \phi(D_{L,M} - D_{L,U}) \tag{19}$$

where σ_{SC} is SC electric conductivity, m_L is the electrophoretic mobility, D_L is the diffusion constant of the drug in the SC lipids. The subscripts *U* and *M* indicate properties associated with the unaltered lipid structure and after full lipid melting, respectively. Much of the overall complexity of this model comes from our use of three interconnected physical processes–heat transfer, electrical current, and mass transfer. All input parameter values are listed in Appendix A.

4 Model Validation

4.1 *Mesh and Time Step Convergence*

In order to mitigate discretization error, we performed mesh convergence analysis. We used a Mapped mesh in the epidermis and SC, which created uniformly small elements in these regions. We used a Free Triangular mesh in the gel and dermis, with a narrow region resolution of 1 and maximum element growth rate of 1.3. In the gel and dermis, meshes had small elements near the boundaries with the pore, epidermis, and SC, and larger elements in the corners far from the SC and epidermis. Our mesh, shown in Figure 5, minimized element size in the areas with the sharpest changes in temperature, electric field, and concentration.

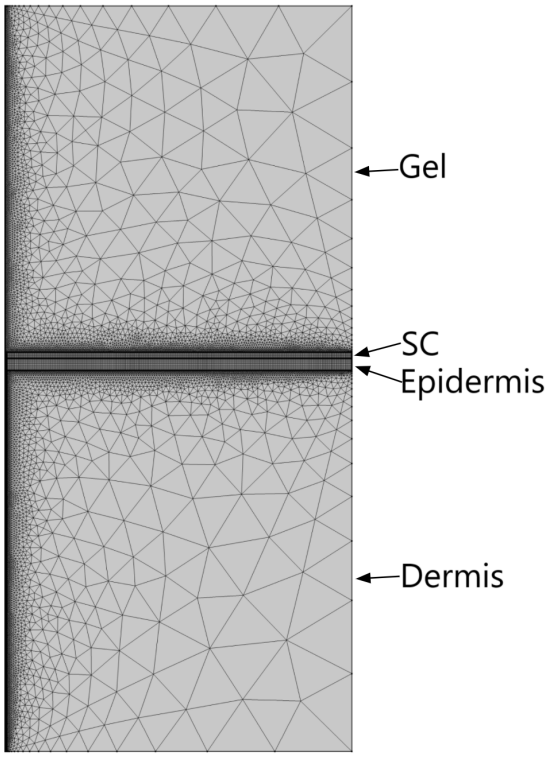

Figure 5. Mesh with variable element size. In the areas with the sharpest changes in temperature, electric field, and drug concentration, element size is minimized. This mesh contains 22,423 elements.

We completed a mesh convergence analysis by plotting the concentration values at 300 ms for 8 different meshes at a point in the SC near the pore, where significant variation in concentration occurs during the first 300 ms. The number of domain elements in each mesh were 1506, 4177, 7057, 10550, 13805, 17327, 22423, and 25091. To create finer meshes, we decreased the Maximum Element Size for the edges of the SC and pore, which decreased the size of the Mapped mesh elements as well as the nearby Free Triangular elements. The concentration

was considered to have converged at the mesh with 22 423 elements, or the second finest mesh. Figure 6 shows the results of the mesh convergence analysis.

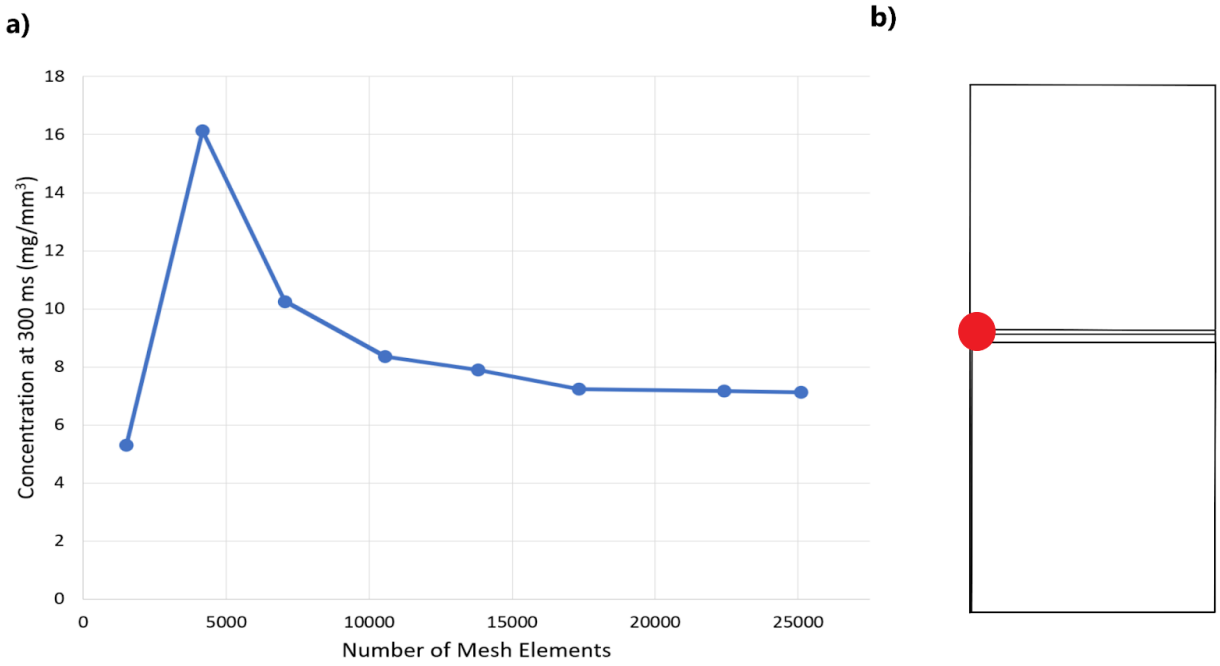

Figure 6. Mesh Convergence Analysis. a) Concentration at a highly varying point in the SC is plotted against the number of mesh elements. The concentration varies by 0.09% between the final two meshes; convergence occurs around 22 500 mesh elements. There is greater concentration variation when there are less mesh elements. As our mesh is more refined, the drug concentration converges at around 22 500. b) The point of interest is shown as a red dot, located in the SC near the pore.

To further reduce discretization error, we performed time step convergence on the chosen mesh. Using Free BDF time stepping, we defined a series of constant maximum step constraints, for values larger and smaller than the maximum time step taken by automatic time stepping. The maximum time steps evaluated were 10 ms, 1 ms, 0.1 ms, 0.05 ms, and 0.01 ms. We evaluated the concentration at the point in the SC near the pore at 300 ms, and there was no change in concentration for any time step evaluated. Thus, the time step was considered to have converged using automatic time stepping, which corresponded to a maximum time step of around 0.1 ms.

4.2 *Computational Validation*

In order to validate our model for times when the electric field was applied, we first compared our results to another study that modeled LTR formation in the SC [11]. This study modeled the same physics as our model, but their geometry differed from our model: the gel-filled pore only passed through the SC, while the pore in our model continues through the epidermis and dermis, which is more realistic for a sweat gland or hair follicle. In order to make the most relevant comparison, we modified our geometry so that the pore passed only through the SC. The modified geometry is shown in Appendix C, Figure 15. We did not change any of the governing equations or boundary conditions, so any validation from this slightly modified model extends to our actual model. The comparison between our model and the data from the study is shown in Figure 7.

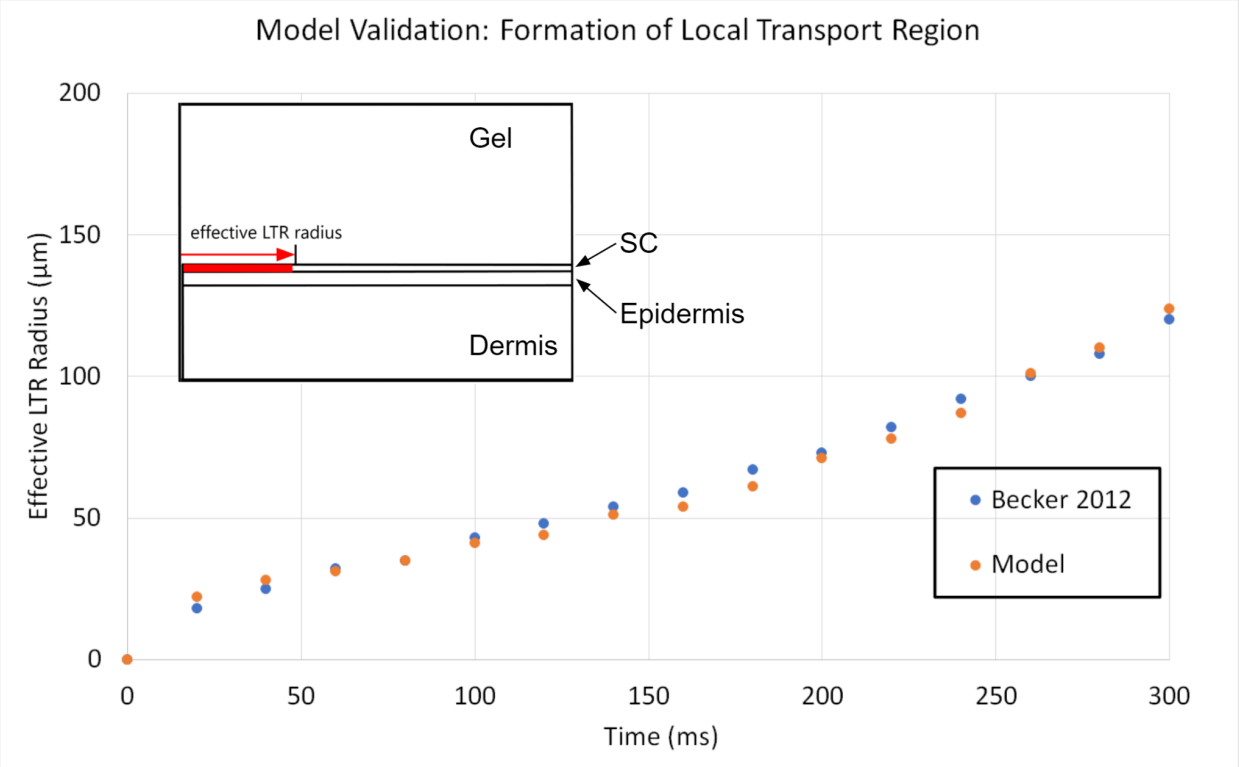

Figure 7. Validation for formation of the local transport region. The effective LTR is a function of time.

When comparing the formation of the LTR, our modified model was validated by this published computational model.

4.3 *Experimental Validation*

To validate our model for longer times based on experimental data, we compared our results to another study that measured transport of calcein through dermatomed porcine skin after electroporation [13]. In this study, a thin layer of skin was placed between two reservoirs of liquid. The reservoir on the SC side of the skin contained the donor solution, with a high initial calcein concentration. The reservoir on the side of the dermis contained the receiver solution, with no initial calcein concentration. Three 45 V pulses were applied across the skin, causing electroporation. The calcein concentration in the receiver solution was measured for 5 hours following electroporation. This experiment also tested a control condition, with the same donor and receiver solutions but no pulse. We modified our model to better match the conditions of the experiment [13]. These modifications changed the values of constants including conductivities and diffusivities, increased the number of pulses to three (with 100 ms gaps in between), decreased the pulse time to 250 ms, decreased the voltage to 45 V, replaced the gel with a donor solution, and added a receiver solution below the dermis layer. The modified model is shown in Appendix C, Figure 16. We adapted our model to the control condition by removing the electric pulse. Figure 8 shows the comparison between our adapted model and the experimental data.

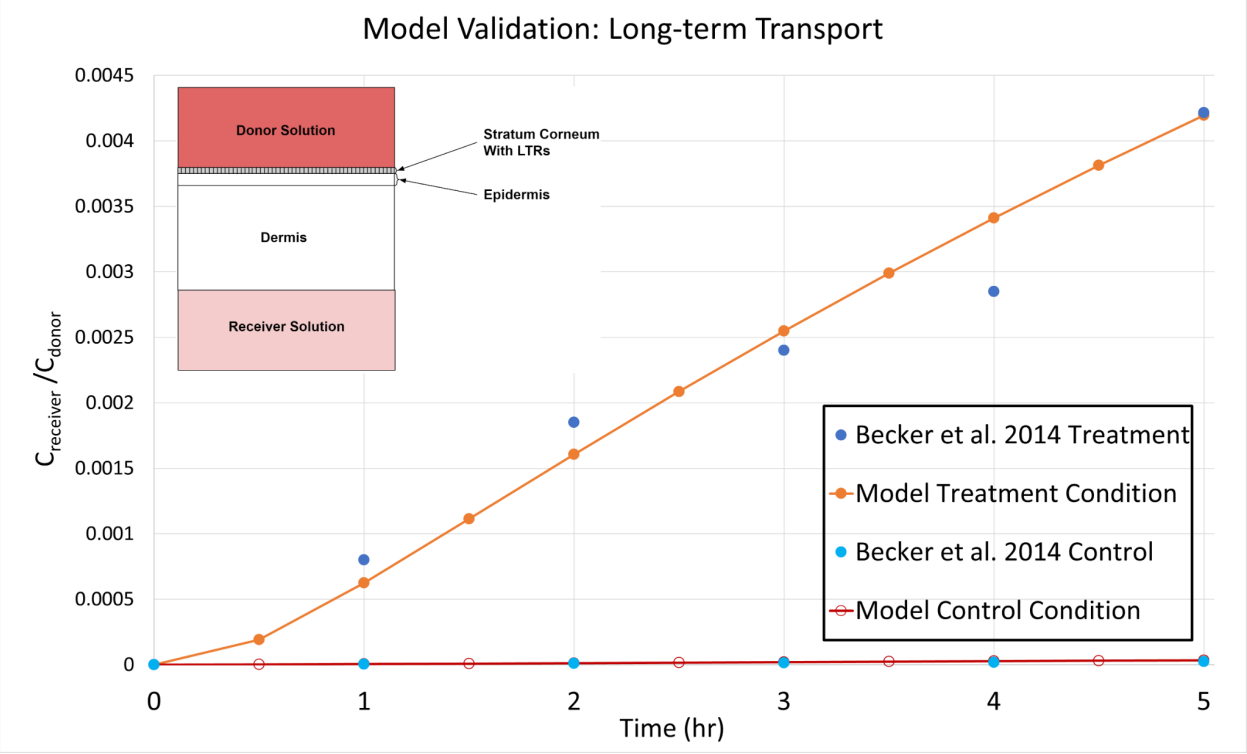

Figure 8. Experimental validation of the concentration profile. The experimental data shows direct measurements of average calcein concentrations. The model calculated the average calcein concentrations. The amount of calcein transported through a single modeled LTR was multiplied by the total number of LTRs on the skin sample, calculated based on skin area and the model's assumption of average pore spacing. The average

concentrations in the modeled donor and receiver solutions were then calculated by dividing the amount of calcein by the solution volume. In the treatment condition, three 45 V and 250 ms pulses were spaced by 100 ms. In the control condition, there was no electric field.

For both the treatment and control conditions, our modified model is validated by the experimental data. Since the underlying physics and governing equations were not changed, the validation of the modified model extends to the actual model.

5 Results

5.1 *Complete Solution*

During the first 300 ms, the electric pulse causes mass transport and LTR formation. Heat transfer, mass transfer, and electric currents are all modeled during this time. The temperature increase in the SC is driven by the Joule heating term in the heat governing equation (Eq 1 & 2). The electrical potential gradient is higher near the pore due to the large difference in electrical conductivity between the gel and the SC, leading to more heating near the gel-SC boundary. Note that as the lipid melts, its electrical conductivity changes, coupling the governing equations for heat transfer and the electric field (Eqs. 1, 2, 6). For this time scale and system, Joule heating has a much larger effect on transient temperature than heat conduction and perfusion. The temperature increase drives lipid melting in the SC, forming the LTR where the lipid has completely melted. Lipid melting is described by Eq. 16. As expected, the LTR develops only near the pore. In regions where lipid melting has occurred, much more mass transfer occurs through the SC. Figure 9 shows the temperature, lipid melt fraction, and concentration profiles near the pore at 300 ms, which allows us to visualize LTR formation.

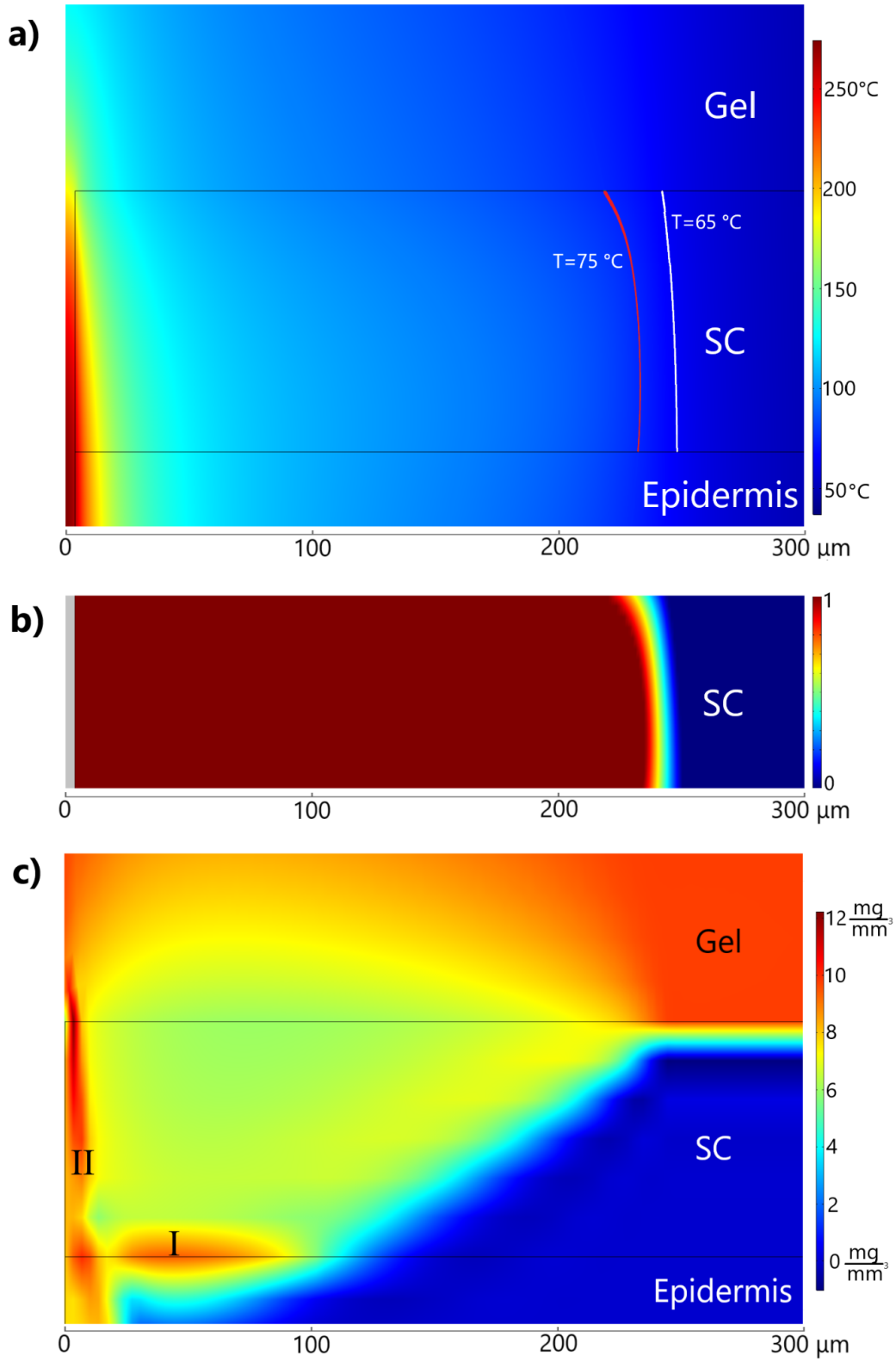

Figure 9. a) Temperature profile at 300 ms, with contours in the SC at temperatures relevant for lipid melting. b) Lipid melt fraction profile in the SC at 300 ms. c) Drug concentration profile at 300 ms, with regions of interest labeled as I and II.

The localized temperature increase in the SC allows the LTR to form. In addition, note that the temperature increase is transient and cooling occurs quickly after 300 ms. From the 75 °C contour in Figure 9a, the region in which full lipid melting has occurred is visible, and at 300 ms this is a radial distance around 230 μm. From the 65 °C contour in Figure 9a, the region in which no lipid melting has occurred is also visible, at a radial distance around 250 μm. There is a steep temperature gradient, creating a sharp transition between the melted and unmelted regions of the SC. Figure 9b shows this transition from fully melted lipid to unmelted lipid, occurring between radial distances of 230 μm and 250 μm. For all further radial distances, no lipid melting has occurred. From Figures 9a and 9b, the LTR can be identified as the circular SC region surrounding the pore with a radius of 240 μm.

LTR formation affects mass transfer through the SC, because the diffusion and electrophoretic mobility coefficients depend on lipid melt fraction. Under normal conditions, the SC is a barrier to mass transport, but diffusion increases when the LTR forms. Figure 9c shows the concentration profile around the LTR immediately after the pulse. There is a sharp concentration gradient at the top of the SC for the region (radial distance above 240 μm) where no lipid melting has occurred, and the SC still has its barrier properties. In the LTR, the concentration gradient is more gradual, especially for radial distances below 240 μm, where the lipid melting has occurred

During the pulse, electrophoretic transport drives the drug along the electric field lines, and diffusive transport drives the drug along its concentration gradient. During this short time period, drug transport is dominated by electrophoretic transport compared to diffusive transport. In the regions near boundaries, electrophoretic transport drives the drug against its concentration gradient, creating regions near boundaries with increased concentrations. Region I occurs because of the difference in electrophoretic mass transport between the SC and epidermis. Because the SC is less electrically conductive than the epidermis by at least an order of magnitude, the main voltage drop is established across the SC and there is a higher voltage gradient within the SC than the epidermis. As shown in equation 11, electrophoretic mass transfer is driven by this voltage gradient, so more transfer occurs within the SC than the epidermis, causing region I to develop near the end of the pulse. Region II occurs because electric field lines near the pore have horizontal components, causing electrophoretic transport horizontal to the pore. Figure 10 shows the concentration gradient every 50 ms during LTR formation, and the evolution of these two regions.

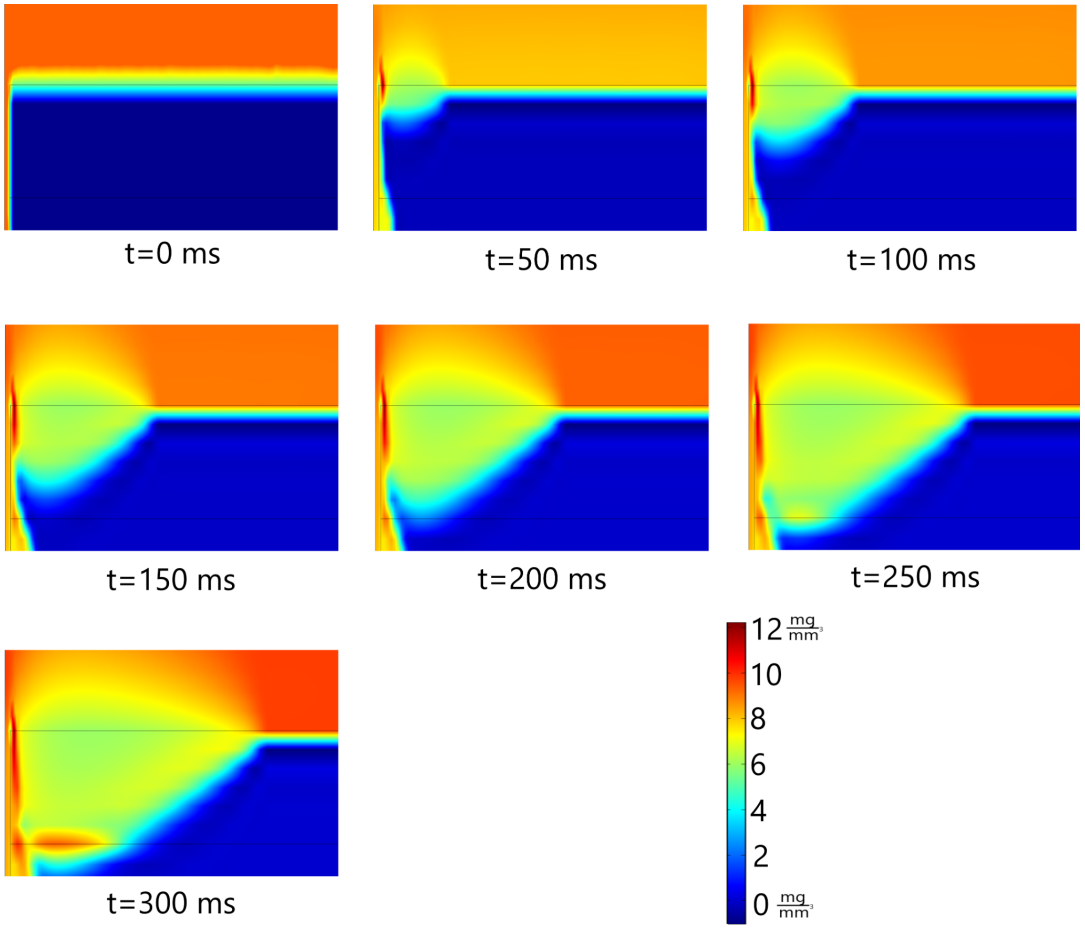

Figure 10. Drug concentration profiles in the LTR during the first 300 ms.

The evolution of the LTR is evident from Figure 10. At early times, lipid melting has only occurred in the region directly adjacent to the pore, and the barrier properties of the SC are evident. As lipid melting occurs, the LTR expands. Around 250 ms, the evolution of region I begins, and the region is also visible at 300 ms as in Figure 9c. This region evolves because of the different voltage gradients in differently conductive skin layers. More mass is transferred by electrophoresis through the melted SC than the epidermis. At 50 ms, the formation of region II can be observed and it continues to evolve as the electric field lines have horizontal components that drive electrophoretic transport of the drug away from the pore.

From Figures 9 and 10, it is clear that LTR formation has occurred during the first 300 ms when the electric pulse has been applied, and that it has significantly increased the amount of mass transfer that occurs through the SC.

After the electric pulse, the LTR remains in the SC, and diffusion through lower skin layers is increased. Since the purpose of the model was to determine the effect of electroporation on drug diffusion at clinically relevant timescales, rather than just during LTR formation, we modeled the diffusive transport that occurs for the 24 hours following the removal of the electrodes. Figure 11 shows the concentration profile at 24 hours.

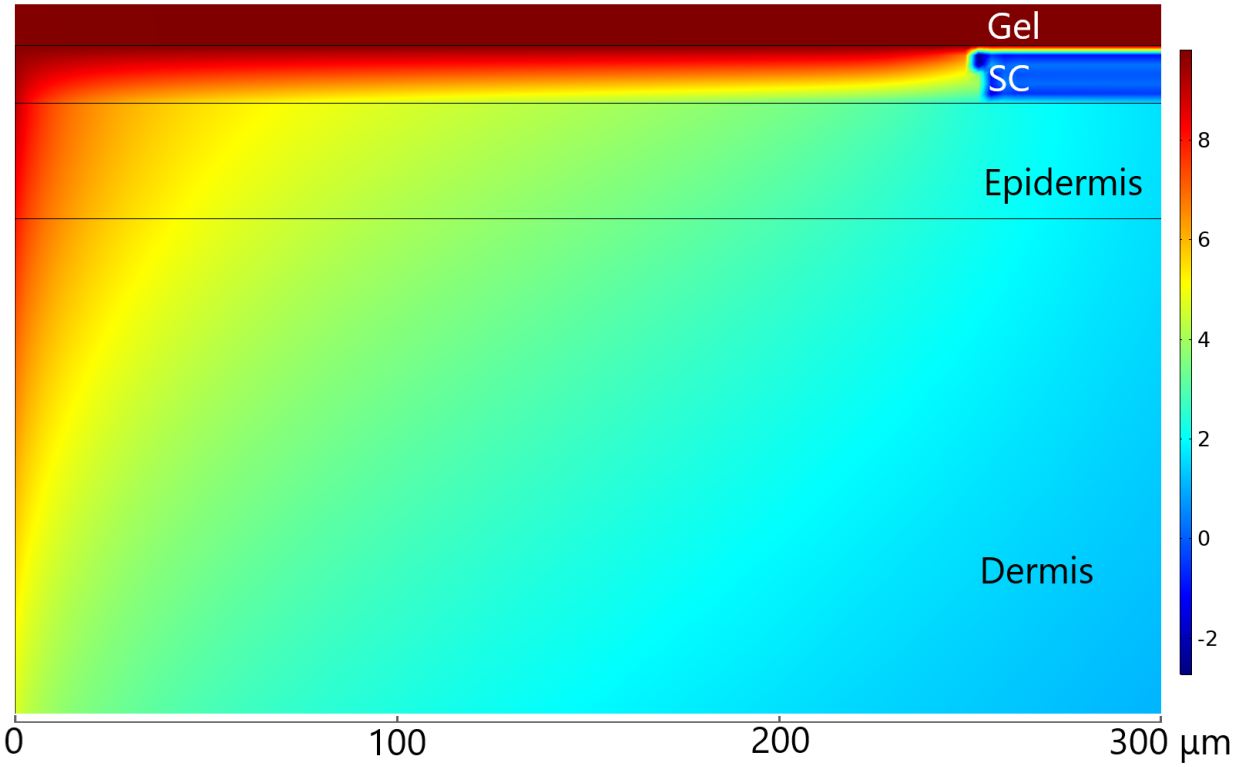

Figure 11. Drug concentration profile around the LTR at 24 hours. Where lipid melting has occurred, the drug has diffused through the SC and into the skin. There is a sharp drop in SC drug concentration for r > 240 µm, where no lipid melting has occurred and the SC still has its barrier properties. Since there is no electric field, this transport is driven by diffusion.

Note that Figures 9 and 11 show the same radial region, but Figure 11 shows more of the skin layers below the SC. This is because the LTR has not changed in size since the end of the pulse, but diffusive transport has driven the drug from the gel into the skin through the LTR. The drug concentration in the epidermis and dermis is much higher than the concentration that would be observed without electroporation. Figure 11 shows that electroporation leads to significant transdermal delivery of the drug after 24 hours have passed.

After it has passed through the SC, the drug enters the bloodstream via the dermis. We selected a point to study within the dermis, for which the concentration was plotted over the whole 24 hours. Transport to this point and on this time scale is dominated by diffusion rather

than electrophoresis. Figure 12 shows the concentration over time and the location of the point selected.

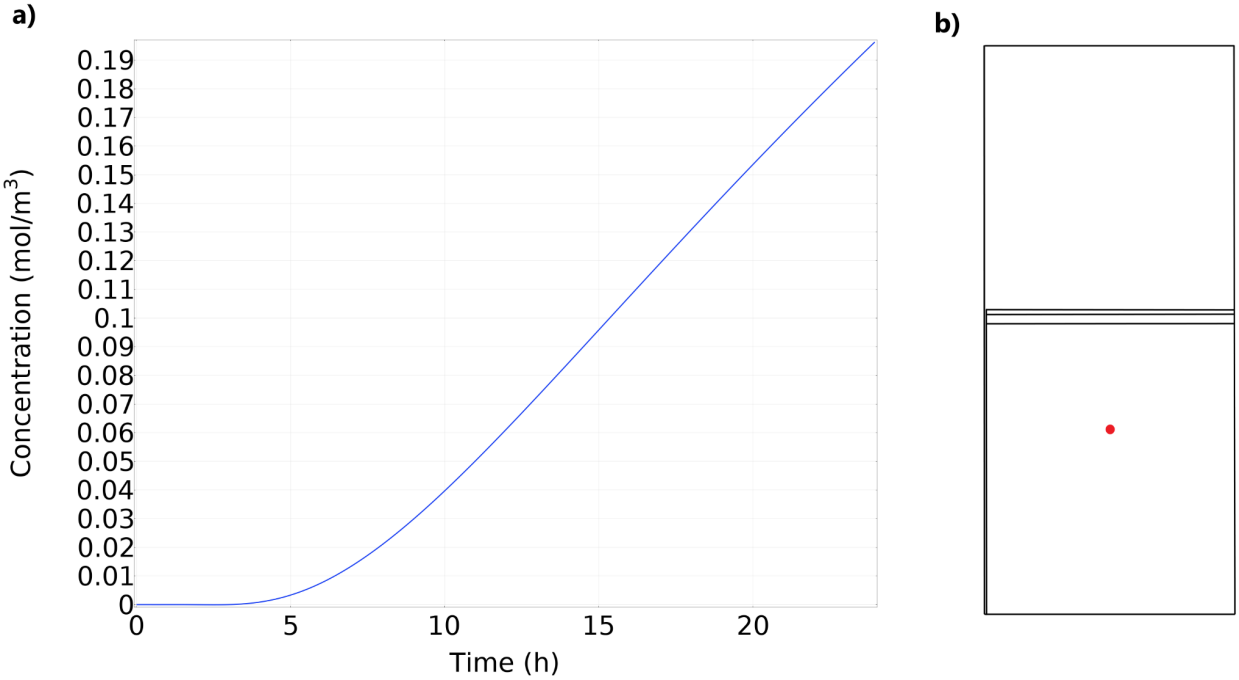

Figure 12. a) Concentration over 24 hours at a central point in the dermis. Drug concentration increases over time as the drug diffuses into the dermis. b) The point of interest is shown as a red dot, located at the center of the dermis.

Electroporation leads to much more transdermal drug delivery than passive diffusion alone, due to the formation of an LTR that disrupts the barrier properties of the SC.

6 Sensitivity Analysis

To analyze the sensitivity of transdermal drug delivery by electroporation, we performed sensitivity analysis. We varied the SC diffusion coefficient, the SC thickness, and the pore radius. These parameters were selected as they could theoretically vary from person to person, and are out of human control--unlike electrical potential, for example. We used range variation for our sensitivity analysis as a distribution approach would take an unfeasible amount of time. We modified each parameter by ±10% and plotted the resulting percent change in concentration of the drug delivered through the SC, compared to that of the original parameter. The results of the sensitivity analysis are shown in Figure 13.

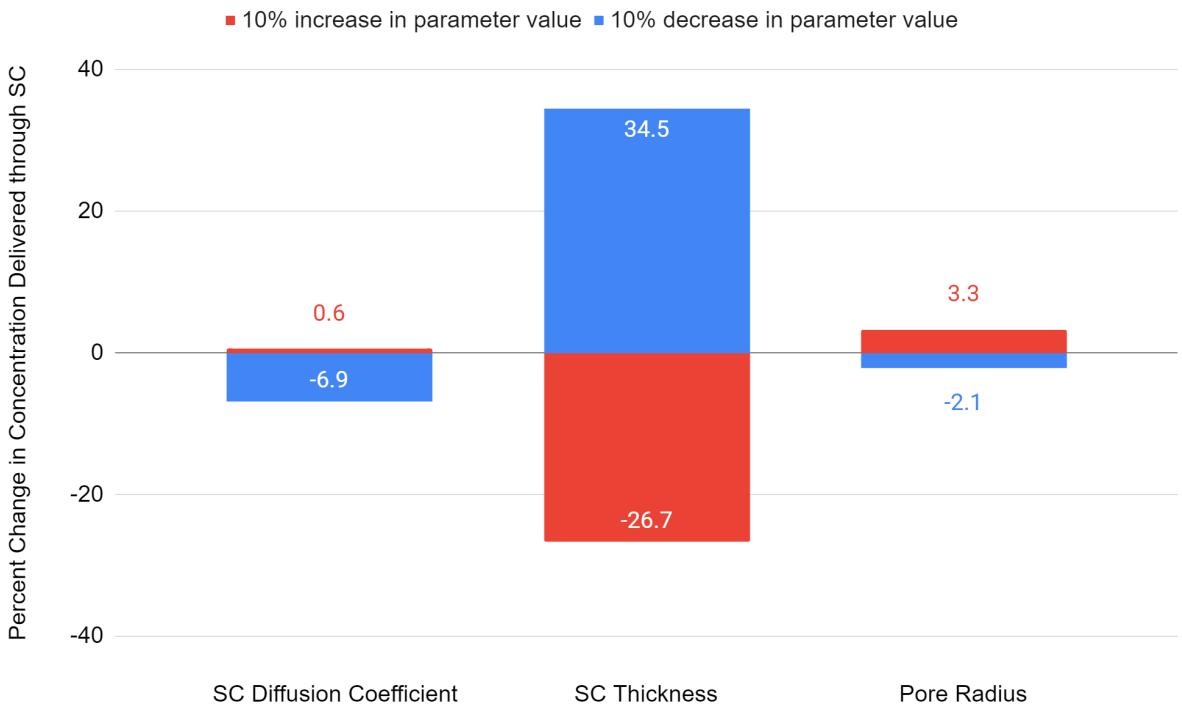

Figure 13. Sensitivity analysis using the SC diffusion coefficient, SC thickness, and pore radius. The total amount of drug that passed through the SC after 24 hours was evaluated for a range of parameter values.

Of the evaluated parameters, drug transport was the most sensitive to SC thickness. A slightly thinner SC allows much more transport, while a slightly thicker SC reduces transport. This is a result of the low diffusion coefficient of the SC. Increasing the diffusion coefficient caused a slight increase in concentration through the SC. The higher diffusion coefficient increases the drug flow through the SC. Similarly, increasing the pore radius caused an increase in concentration through the SC, as a larger pore contains more gel, allowing for more drug transfer below the SC via the gel.

7 Conclusion

The purpose of our study was to model the effect of electroporation on the diffusion of a DNA drug through the skin over a span of 24 hours. In the first 300 ms, an electric pulse caused increased transport of the charged particles through electrophoresis, and melted the lipids in the SC via Joule heating, forming an LTR. At the end of the pulse, the LTR stopped changing in size, and diffusion became the only relevant form of transport.

In accordance with our objectives, we modeled the first 300 ms during the pulse and the 24 hours that followed. Our results show that the concentration of drug at 24 hours decreases greatly going down the LTR in the SC, with a slower decline in the epidermis and dermis. These results make sense, as even when its lipids have melted, the SC still has the lowest diffusivity of the skin layers. To further validate, our mesh and time step convergences show that discretization error did not significantly impact our results. We also modified our model to mirror another electroporation model and an in vitro experiment, both of which validated our model.

Sensitivity analysis showed that variation in SC thickness had a sizable impact on the amount of drug that diffused through the SC in 24 hours. SC diffusivity variation and pore radius variation had less notable effects, comparatively. This result reinforces the importance of the SC as a barrier layer to the skin, and the fact that any transdermal drug delivery method must bypass the SC.

Our model produces valid results for realistic scenarios. We have successfully closed a gap in existing literature by modeling transdermal drug delivery with electroporation, in human tissue for times extending beyond the duration of the electric pulse. In addition, we have demonstrated that electroporation could be a useful method to deliver DNA drugs. We believe that our model could be used as a proof of concept before clinical studies, specifically for electroporation on human skin. Further analysis should focus on modifications to the timing and voltage of electric pulses and the corresponding effects on the maximum temperature reached in the SC. This analysis could be combined with data about skin temperature and short-term heating sensations, to ensure that this drug delivery method is truly painless, as we expect it to be. To further validate our model, future experiments should involve *in vivo* testing on human skin through clinical trials. Our model's property values are based on *in vitro* studies of polyacrylamide and agarose gels, which have properties slightly different from human skin.

In the context of design, this model allows us to easily test parameter changes that would be time-consuming and expensive to test through experiments. The underlying physics of the model are not dependent on the use of a DNA drug. With experimental values for the diffusivity and electrophoretic mobility of any drug in skin, this model can be used to determine the efficacy of transdermal drug delivery of that drug via electroporation.

7.2 *Design Constraints and Considerations*

The device should be designed so that it can be manufactured quickly and easily. The design reflected in our model reflects this: the most complex components are the electrodes, which are already widely used in commercially available electronics. The manufacturing process for the device modeled here will not be extremely complex. Further design work should focus on making the device accessible to patients, so that drug delivery does not require a specifically trained medical professional. Since an ideal device would be used at a patient's home, the system must be easy to use. To maintain safety and efficacy, it is important that the drug is delivered consistently. Thus, the gel patch that contains the drug should be standardized. The amount of drug in the hydrogel should be constant, and the gel should fit over the electroporated area so that there is not excess gel over impermeable skin. The mechanism that gathers the skin fold and holds it in place during the pulse should be easy to use, so that it takes the same amount of skin each time, standardizing the average potential gradient. In addition, the device should include a variable power supply so that it can plug into any wall outlet. The device should be designed to compete with other effective and inexpensive transdermal delivery devices such as microneedle patches.

The device that can be designed from this model has further advantages in terms of environmental sustainability. Transdermal drug delivery is an alternative to injections, which require syringes. Disposable syringes result in an immense amount of carbon emissions every year, which is highly damaging to the environment. Commercially available syringes are made of plastic, stainless steel, and glass. Microneedle-based delivery systems also produce wastes in the form of plastic and the metal that the microneedles themselves are made of. On the other hand, the only waste from electroporation involves the used hydrogel. By carefully designing the dimensions of the hydrogel, waste can be minimized - ideally so that this system produces less waste than an injection-based or microneedle delivery system.

A device that is able to reduce environmental waste also has more economic advantages. The electrode should be reusable for repeated drug delivery. By optimizing an electrode for a long life span, there will be economic advantages for using transdermal drug delivery over repeated use of disposable syringes. In tying back to the manufacturing process, further research is needed to reduce the device cost.

The product design process will need to be ethically sound, by minimizing risks to health and safety. *In vivo* human trials will be required in the early stages of product design, and these studies should be conducted ethically and carefully. The goal of these studies will be to ensure that electroporation by this method is painless, and that cell damage does not occur. Once the system has been approved for patient use, injuries are most likely to be caused by the electrical components. The device should be designed so that it cannot deliver pulses longer than 300 ms, and it cannot deliver frequent pulses. The variable power supply should also be designed so that it cannot provide voltages that would be damaging to human skin.

8 Appendix A: Mathematical Statement of the Problem

Table 1: Variables

solute concentration	C
joule heating	Q_J
temperature	T
electric potential	Φ
SC lipid melt fraction	ϕ

Table 2: Properties Varying by Skin Layer

Property	**Variable**	**Units**	**Gel**	**SC**	**Epidermis**	**Dermis**
perfusion	ω	kg/m^3s	0	0	0	2.33
specific heat	$c_{p,i}$	J/kgK	4180	3600	3600	3800
thermal conductivity	k_i	W/mK	0.6	0.2	0.209	0.293
density	ρ_i	kg/m^3	1000	1500	1110	1116
electrical conductivity	σ_i	S/m	1.5	$\sigma_{SC,U} = 10^{-5}$ $\sigma_{SC,M} = 10^{-3}$	0.01	0.015
electrophoretic mobility	m_i	m^2/Vs	10^{-8}	$m_{L,U} = 2.67 \cdot 10^{-14}$ $m_{L,M} = 5.96 \cdot 10^{-8}$	10^{-10}	$2 \cdot 10^{-10}$
diffusion coefficient	D_i	m^2/s	10^{-9}	$D_{L,U} = 8.9 \cdot 10^{-17}$ $D_{L,M} = 1.99 \cdot 10^{-10}$	10^{-12}	10^{-12}

Properties in Table 2 are from reference [12].

Table 3: Constant Input Parameters

Parameter	Variable	Value
specific heat of blood	c_b	3800 J/kgK
arterial blood temperature	T_a	37℃
initial drug concentration	C_0	0.1 mg/mm^3
ambient temperature	T_∞	20°C
temperature at which SC lipid phase change is initiated	T_{E1}	65℃
temperature at which SC lipid structure is fully altered	T_{E2}	75℃
porosity of the SC	ε_{SC}	0.00249
tortuosity of the SC	τ_{SC}	8.57
convective heat transfer coefficient	h	15 W/m^{2}K

Properties in Table 3 are from reference [12].

9 Appendix B: Solution Strategy

MUMPS direct solver was used to solve the algebraic equations. Free BDF time stepping was used. Relative tolerance was 10^{-6}, absolute tolerance factor was 1000. Figure 14 shows the CPU time taken and memory used by a typical run during the electric pulse.

```
4044         0.3  4.9862e-06     7403  773 7403     1   123      0  4.3e-15  4.3e-16
4045         0.3  2.4931e-06     7406  775 7406     1   124      0  1.9e-15    4e-16
4046         0.3  1.2465e-06     7409  777 7409     1   125      0  2.3e-15  3.9e-16
4047         0.3  1.5582e-07     7414  780 7414     1   127      0    7e-16  3.6e-16
4048         0.3  1.5627e-07     7417  782 7417     1   128      0  4.7e-16  5.1e-16
4049         0.3  7.8134e-08     7420  784 7420     1   129      0  3.3e-16  3.7e-16
   -         0.3           - out
4050         0.3  4.9104e-08     7424  786 7424     1   130      0    4e-16  5.4e-16
Time-stepping completed.
Solution time: 2778 s. (46 minutes, 18 seconds)
Physical memory: 1.95 GB
Virtual memory: 2.49 GB
```

Figure 14. COMSOL output showing time stepping and memory used by a typical run.

10 Appendix C: Additional Visuals

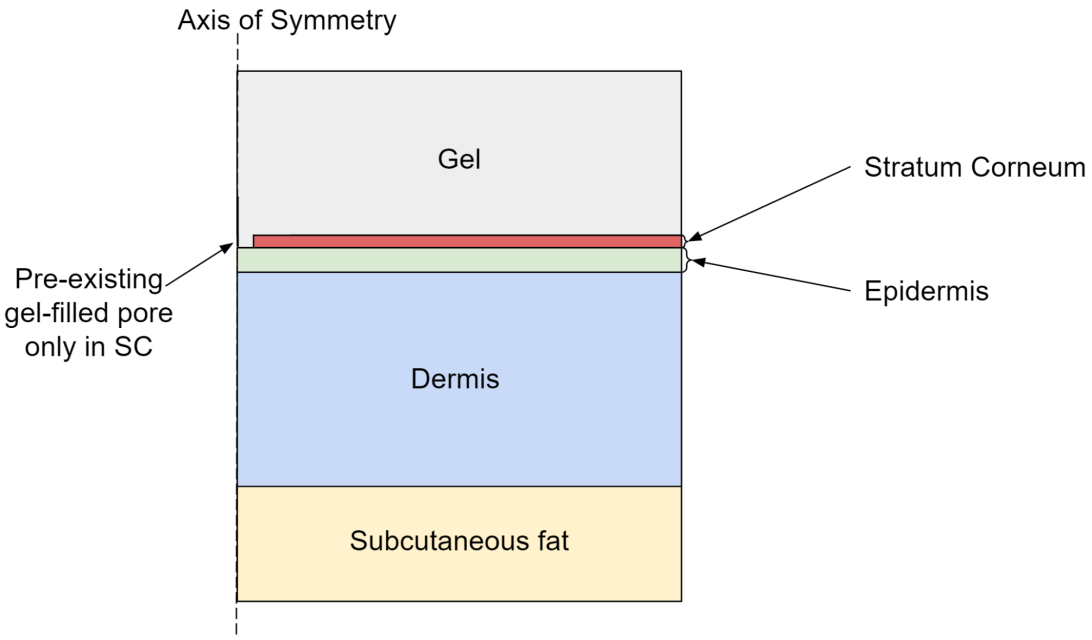

Figure 15. Modifications to geometry used for computational validation. The pre-existing pore occurs only in the SC. This geometry was used only for validation.

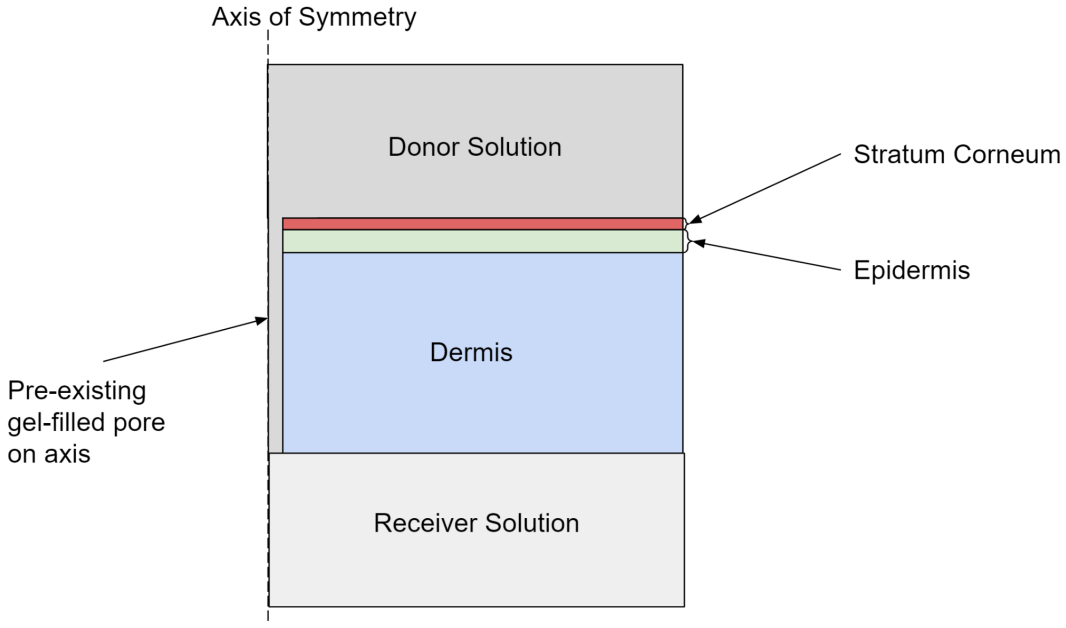

Figure 16. Modifications to geometry used for experimental validation. There is a receiver solution beneath the dermis. This geometry was used only for validation.

11 Appendix D:

References

[1] A. Savoca, G. Mistraletti, and D. Manca, “A physiologically-based diffusion-compartment model for transdermal administration – The melatonin case study,” Computers & Chemical Engineering, vol. 113, pp. 115-124, 2018. doi: 10.1016/j.compchemeng.2018.03.008.

[2] A. Z. Alkilani, M. T. C. McCrudden, and R. F. Donnelly, “Transdermal Drug Delivery: Innovative Pharmaceutical Developments Based on Disruption of the Barrier Properties of the Stratum Corneum,” *Pharmaceutics*, vol. 7, no. 4, pp. 438–470, 2015. doi: 10.3390/pharmaceutics7040438

[3] C. M. Schoellhammer, D. Blankschtein, and R. Langer, “Skin permeabilization for transdermal drug delivery: recent advances and future prospects,” *Expert Opinion on Drug Delivery*, vol. 11, no. 3, pp. 393–407, 2014. doi: 10.1517/17425247.2014.875528

[4] D. Ramadon, M. T. McCrudden, A. J. Courtenay, and R. F. Donnelly, “Enhancement strategies for transdermal drug delivery systems: Current trends and applications,” Drug Delivery and Translational Research, 2021. doi: 10.1007/s13346-021-00909-6

[5] J. Dermol-Černe and D. Miklavčič, "From Cell to Tissue Properties—Modeling Skin Electroporation With Pore and Local Transport Region Formation," IEEE Transactions on Biomedical Engineering, vol. 65, no. 2, pp. 458-468, Feb. 2018, doi: 10.1109/TBME.2017.2773126.

[6] J. J. Escobar-Chávez, D. Bonilla-Martinez, M. A. Villegas-González, I. M. Rodríguez-Cruz, and C.L. Domínguez-Delgado, “The Use of Sonophoresis in the Administration of Drugs Throughout the Skin,” Journal of Pharmacy and Pharmaceutical Sciences, Feb. 2009. doi: 10.18433/J3C30D.

[7] K. Kretsos and G. B. Kasting, “A geometrical model of dermal capillary clearance,” *Mathematical Biosciences*, vol. 208, no. 2, pp. 430–453, 2007. doi: 10.1016/j.mbs.2006.10.012

[8] M. R. Prausnitz and R. Langer, “Transdermal drug delivery,” *Nature Biotechnology*, vol. 26, no. 11, pp. 1261-1268, 2008. doi: 10.1038/nbt.1504

[9] M. Roustit, S. Blaise, and J. Cracowski, “Trials and tribulations of skin iontophoresis in therapeutics,” *British Journal of Clinical Pharmacology*, vol. 77, no. 1, pp 63-71, 2013. doi: 10.1111/bcp.12128.

[10] N. Pavšelj and V. Préat, “DNA electrotransfer into the skin using a combination of one high- and one low-voltage pulse,” Journal of Controlled Release, vol. 106, no. 3, pp. 407 - 415, September 2005. doi: 10.1016/j.jconrel.2005.05.003

[11] R. Vanbever, M.-A. Leroy, and V. Préat, “Transdermal permeation of neutral molecules by skin electroporation,” Journal of Controlled Release, vol. 54, no. 3, pp. 243–250, 1998. doi: 10.1016/s0168-3659(97)00146-6

[12] S. Becker, “Transport modeling of skin electroporation and the thermal behavior of the stratum corneum,” International Journal of Thermal Sciences, vol. 54, pp. 48-61, April 2012. doi: 10.1016/j.ijthermalsci.2011.10.022

[13] S. Becker, B. Zorec, D. Miklavčič, and N. Pavŝelj, “Transdermal transport pathway creation: Electroporation pulse order,” Mathematical Biosciences, vol. 257, pp. 60-68, 2014. doi: 10.1016/j.mbs.2014.07.001

12 Team Responsibilities

Team member name	James Adair	Emily Chou	Matt Metzloff	Truman Tse	NOT DONE
Wrote abstract				x	
Edited abstract	x	x	x		
Wrote introduction	x	x	x	x	
Edited introduction	x	x	x	x	
Wrote method section		x	x	x	
Edited method section	x	x	x	x	
Wrote results section	x	x	x		
Edited results section	x	x		x	
Wrote discussion section (validation)	x		x		
Edited discussion section (validation)	x	x	x	x	
Wrote summary and conclusion section	x		x		
Edited summary and conclusion section		x	x	x	
Wrote bibliography section	x	x		x	
Edited bibliography section		x		x	
Prepared processed data table for appendix		x		x	
Checked data in processed data table in appendix	x	x	x	x	
Prepared figures or tables for main text			x		
Checked figures or tables in main text	x	x		x	
Assigned tasks to group members	x	x	x	x	
Put the report together from the parts provided by others	x	x	x	x	
Read and edited entire document to check for consistency	x	x	x	x	
Conducted literature search	x	x	x	x	
Ran COMSOL trials	x		x		